Determination of the 2*s*-2*p* excitation energy of lithiumlike scandium using dielectronic recombination

Stefan Kieslich, Stefan Schippers, Wei Shi,* and Alfred Müller
Institut für Atom- und Molekülphysik, Justus-Liebig-Universität, 35392 Giessen, Germany

Gerald Gwinner,† Michael Schnell, and Andreas Wolf
Max-Planck-Institut für Kernphysik, 69117 Heidelberg, Germany

Eva Lindroth and Maria Tokman
Atomic Physics, Fysikum, Stockholm University, S-106 91 Stockholm, Sweden
(Received 22 April 2004; published 22 October 2004)

High-resolution spectroscopy of doubly excited states produced by dielectronic recombination (DR) of lithiumlike Sc^{18+} ions was performed by employing the electron-ion merged-beam technique at the heavy-ion storage ring TSR. The experimental procedure for measuring DR resonances with high precision is thoroughly described with an emphasis on the uncertainties of the experimental energy scale. Absolute measurements of recombination rate coefficients were carried out over the center-of-mass energy range 0–50 eV that comprises all DR resonances associated with $2s_{1/2} \rightarrow 2p_{1/2,3/2}$ excitations. At relative energies below 300 meV resonances due to DR via Sc^{17+} $(1s^2\ 2p_{3/2}\ 10l_j)$ intermediate states were found. Their positions could be measured with an uncertainty of only ±1.8 meV. The results are compared with theoretical calculations within the framework of relativistic many-body perturbation theory. By combining the precision of the experimental and theoretical results we derive a value for the $2s_{1/2} \rightarrow 2p_{3/2}$ excitation energy, 44.3107(19) eV, which is by more than an order of magnitude more accurate than the hitherto most precise value obtained from optical spectroscopy.

DOI: 10.1103/PhysRevA.70.042714 PACS number(s): 34.80.Lx, 36.20.Kd

I. INTRODUCTION

Electron-ion recombination experiments employing the merged-beam technique at heavy-ion storage rings equipped with electron coolers are particularly sensitive to dielectronic recombination (DR) resonance energies and widths in the region of matching electron and ion velocities, i.e., near zero relative energy [1,2]. These experiments, therefore, bear a potential for high-resolution spectroscopy of doubly excited states provided that the atomic system under study exhibits DR resonances at very low energies. In this type of spectroscopy the binding energy of a Rydberg electron serves as a high-accuracy probe for inner-electron excitation energies. Here we explore the experimental and theoretical prerequisites of such a technique, aiming at a precision determination of excitation energies in highly charged few-electron systems with accuracies of the order of 1 meV over a wide range of ion charges as an alternative to optical spectroscopy. In particular, we consider the determination of the 2*s*-2*p* excitation energy in lithiumlike ions. A favorable case with very low-lying DR resonances is the system Sc^{18+}.

DR of lithiumlike ions is especially attractive since the atomic structure on one hand is relatively simple so that the doubly excited berylliumlike DR resonance states can still be identified. On the other hand, they present an interesting case where many-body, relativistic, and QED (quantum electrodynamical) effects have to be included in a theoretical description [4–8] that tries to match the available experimental precision. The relative importance of relativistic and QED effects increases with increasing nuclear charge *Z*. In order to test state-of-the-art electron-ion recombination and atomic structure theory, it is therefore of interest to study a high-*Z* lithiumlike system that exhibits DR resonances at very low energies, where the experimental resolution is the highest. So far, the lowest-lying DR resonance that has been individually resolved was found in lithiumlike F^{6+} at about 10 meV [3].

A simple calculation of DR resonance energies E_n with the Bohr formula

$$E_n = E_{3/2}^{\infty} - R\left(\frac{q}{n}\right)^2 \tag{1}$$

for Rydberg binding energies predicts the existence of low-energy Sc^{17+} $(1s^2\ 2p_{3/2}\ 10l_j)$ resonances. With the $2s_{1/2} \rightarrow 2p_{3/2}$ excitation energy $E_{3/2}^{\infty} = 44.31$ eV [9], the Rydberg constant $\mathcal{R} = 13.606$ eV, the initial ion charge $q = 18$, and the Rydberg quantum number $n = 10$, Eq. (1) yields $E_{10} \approx 0.23$ eV.

Based on this expectation, the goal of the present study, in addition to the measurement of DR rate coefficients for Sc^{18+} ions, is high-resolution spectroscopy of the $Sc^{17+}(1s^2\ 2p_{3/2}\ 10l_j)$ DR resonances and comparison of the experimental results with calculations in the framework of relativistic many-body perturbation theory (RMBPT) in all-order formulation and taking into account radiative QED corrections to the lowest order. The treatment of radiative ef-

*Present address: Department of Physics,University of Florida, Tallahassee, FL, USA.

†Permanent address: Department of Physics and Astronomy, University of Manitoba, Winnipeg, MB, Canada R3T 2N2.

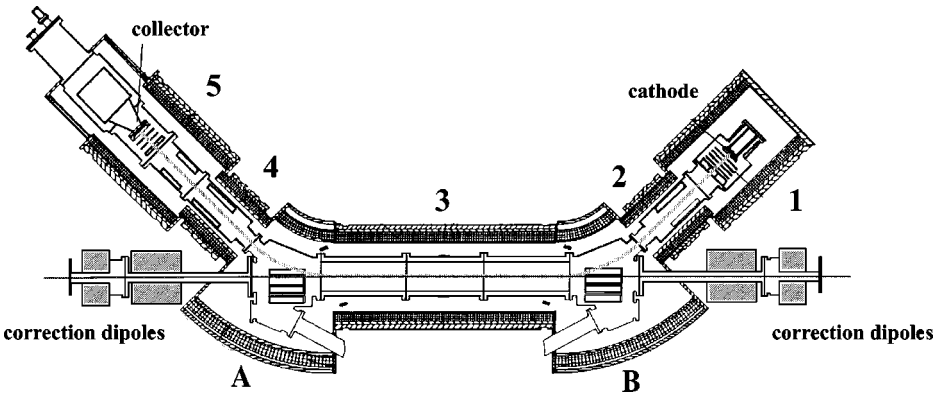

FIG. 1. Schematic picture of the electron cooler in the Heidelberg storage ring TSR. The magnetic field that guides the electron beam is generated by five solenoid (marked $1,2,\ldots,5$) and two toroid (marked A,B) magnets. Additional dipole coils on top of the solenoid magnets allow for an exact positioning of the electron beam.

fects, such as self-energy and vacuum polarization, in a many-electron environment is a field that is still in a development phase. From this point of view the present Z region, where both many-body and QED effects are important, is of special interest. RMBPT calculations have already successfully described the low-energy resonances found in DR of the light lithiumlike ions C^{3+} [4] and F^{6+} [5] as well as in the heavy copperlike ion Pb^{53+} [10] and have also been used to calculate Ar^{15+} [6] and Kr^{33+} [7] DR resonances at somewhat higher energies where the experimental resolution is lower and where correlation effects are thus less critical for the comparison.

The present work is particularly devoted to a systematic assessment of the potential of storage-ring recombination experiments as an alternative spectroscopic approach in competition with optical techniques. In the course of investigating and further developing this potential we use DR resonance spectroscopy to find a new value for the $2s_{1/2} \rightarrow 2p_{3/2}$ excitation energy in the lithiumlike Sc^{18+} ion. This is done by combining the high-accuracy measurement of resonance positions with a calculation of the binding energy of the captured electron. The fact that the outer electron is in a high-n state allows for a calculation of its binding energy relative to the excited target that is precise enough not to influence the overall accuracy in the $2s_{1/2}-2p_{3/2}$ energy determination at the present level of experimental accuracy.

The paper is organized as follows. A discussion of the experimental procedure focusing especially on the accuracy of the experimental energy scale is presented in Sec. II. The theoretical RMBPT treatment is detailed in Sec. III. The experimental and theoretical results are presented and discussed in Sec. IV. Summarizing conclusions are given in Sec. V.

II. EXPERIMENT

The beam of $^{45}Sc^{18+}$ ions was supplied by the tandem-booster facility of the Max-Planck-Institut für Kernphysik in Heidelberg, Germany. The ions were accelerated to an energy of 176.4 MeV and passed through a stripper foil to obtain the required ion charge state $q=18$. Subsequently, they were injected into the storage ring. The ion current in the storage ring was enhanced by using multiturn injection and ecool stacking [11]. With this technique beams with intensities up to almost 80 μA at an energy of 3.9 MeV/u were obtained. The ion beam was cooled by the interaction with a velocity-matched cold beam of magnetically confined electrons in the cooling device. In order to satisfy the velocity-matching condition an electron beam laboratory energy of fulfill the velocity matching condition an electron beam laboratory energy of 2.152 keV was required. In the following this energy is referred to as the "cooling energy" E_c.

The electrons in the cooling device (electron cooler, Fig. 1) were emitted from a thermal cathode at temperature $T_c \approx 1200$ K and then accelerated to the desired energy. As a result of the acceleration the longitudinal electron energy spread, i.e., the energy spread in beam direction, was largely reduced. In order to prevent the electron beam from being blown up by its own space-charge electrical field it was magnetically guided on its entire path through the electron cooler. The transverse electron energy spread was reduced by adiabatically passing the ions [12–14] from an initial region of high magnetic field $B_c \sim 1$ T to a region of lower magnetic field $B=B_c/\zeta$. In the present experiment the factor ζ was varied from 9.6 up to 25. The magnetic guiding field B was kept constant throughout the remaining part of the electron cooler, including the toroidal merging and demerging sections, as well as the straight section where electron and ion beams overlap. The electron density was $n_e=1.21 \times 10^7$ cm^{-3} at cooling energy and varied proportionally to the electron energy.

Special care was taken to center the two beams correctly with respect to each other over the entire interaction length by steering the electron beam with the aid of dipole field coils mounted inside each of the electron cooler's solenoids. Due to its much larger rigidity the ion beam is nearly unaffected by the steering. With both beams well centered, electric fields in the frame of the ions originating from the space-charge and motional $(\vec{v}\times\vec{B})$ fields are estimated to be less than 10 V/cm [15].

In the first dipole bending magnet downstream from the electron cooler the recombined Sc^{17+} ions were separated from the parent Sc^{18+} beam and detected with a single-particle scintillation counter (with nearly 100% detection efficiency) [16]. Normalization on both the electron density n_e and the number N_i of ions in the storage ring yields the rate coefficient on an absolute scale:

$$\alpha = \frac{R}{N_i n_e \eta} \frac{C}{L} \gamma_i^2, \tag{2}$$

where R is the background-corrected [17] counting rate of the recombined Sc^{17+} ions, $\eta = 1.0^{+0.00}_{-0.03}$ is the detector efficiency, $C = 55.4$ m is the circumference of the storage ring, $L = 1.5$ m is the length of the interaction zone, and the factor γ_i^2 originates from the relativistic transformation between the laboratory frame and the rest frame of the ions. The systematic error for the measured absolute rate coefficient is ±15% [18]. It stems from uncertainties of the detector efficiency, the ion and electron current measurement, and the beam overlap.

A. Accuracy of the energy scale

The accurate determination of the electron-ion collision energy E_{rel} is crucial for comparisons between experiment and theory. Experimentally, $E_{\mathrm{rel}} \neq 0$ is achieved by periodically shifting the electron energy E_e away from the cooling energy, which defines the ion energy E_i. In turn, E_i remains nearly unchanged during these periods due to the large inertia of the ions. This enables us to measure recombination rate coefficients at well-defined values of E_{rel}. In order to determine E_{rel}, which is defined in the electron-ion center-of-mass (c.m.) frame, a relativistic transformation of the laboratory frame is performed according to

$$E_{\mathrm{rel}} = m_i c^2 (1+\mu)[\sqrt{1 + 2\mu(1+\mu)^{-2}(G-1)} - 1] \tag{3}$$

with the (electron-ion) mass ratio $\mu = m_e/m_i$ and with

$$G = \gamma_i \gamma_e - \cos\theta \sqrt{(\gamma_i^2 - 1)(\gamma_e^2 - 1)}, \tag{4}$$

where $\gamma_i = 1 + E_i/m_i c^2$ and $\gamma_e = 1 + E_e/m_e c^2$; θ is the laboratory angle between the electron and the ion beam, and E_i (E_e) and m_i (m_e) are the kinetic energy and the rest mass of the ions (electrons), respectively. While this form is used in the actual data reduction, the nonrelativistic expression

$$E_{\mathrm{rel}}(\theta = 0) \approx \left(\sqrt{E_e} - \sqrt{\frac{m_e}{m_i} E_i} \right)^2 \tag{5}$$

is much more intuitive and sufficiently accurate for a general discussion of errors in the energy calibration.

The knowledge of the masses m_i and m_e of ions and electrons, respectively, poses no problem, and the determination of the collision energy boils down to controlling E_e, E_i, and θ in the laboratory frame. Before discussing the systematic uncertainties connected with these quantities, some remarks about the peculiarities of the merged-beam method with electron-cooled ions are in order to illustrate the precision and robustness of dielectronic recombination measurements, particularly at low E_{rel}.

At a first glance, Eq. (5) implies that working at small relative energies involves an unappealing procedure, the subtraction of two very similar, large numbers. However, under the present experimental conditions the determination of E_{rel} can be reduced to the precise knowledge of the difference $\Delta E = E_e - E_c$ which results from an additional acceleration (or deceleration) of the electrons beyond the cooling energy. Measurement periods are interleaved with electron cooling intervals, characterized by the electron energy E_c. The electron-ion interaction forces the ions to an energy $E_i = (m_i/m_e)E_c$. If the ensuing measurement period is sufficiently short, E_i does not change significantly (the validity of this assumption is discussed below). In fact we can rewrite Eq. (5) as $E_{\mathrm{rel}} \approx (\sqrt{E_c + \Delta E} - \sqrt{E_c})^2$ and for $\Delta E \ll E_c$ we arrive at

$$E_{\mathrm{rel}} \approx \frac{(\Delta E)^2}{4E_c}. \tag{6}$$

It is much simpler to measure the voltage jump $\Delta U = \Delta E/e$ of the electron cooler between cooling and measuring periods than to determine ion and electron energies separately. Since E_c enters Eq. (6) as a factor, any uncertainty in E_c has a vanishing influence on the uncertainty of the relative energy scale (and, correspondingly, a small influence on E_{rel}) as long as E_{rel} is small. E_c can be stabilized to 1×10^{-4} and hence [according to Eq. (6)] E_{rel} has similar relative accuracy. It should be noted that this kind of self-calibration of the system stems from the principle of electron cooling and is a tremendous advantage of storage ring work over single-pass schemes; variations in the ion energy caused by the accelerator during a measurement cancel completely.

In the following we will discuss the influence of several effects on the determination of E_c and ΔE. The emphasis is on the lowest-energy resonance observed in the experiment at about 70 meV.

1. Space-charge of the electron beam

Experimentally, one measures the negative potential of the cathode where the electrons are created. The merged-beam section is contained in a grounded beam pipe. The ion beam is much smaller in diameter than the electron beam and is traveling along the axis of the latter. As the surrounding electrons produce a space charge, the ions interact with electrons of diminished energy, and a space-charge correction has to be applied to obtain E_c from the measured cathode potential. In the present experiment the potential difference between the grounded beam pipe and the axis of the electron beam is 233 V at cooling energy, about 10% of the cathode potential. Furthermore, as the electron density varies with the cathode voltage, the space-charge correction also is a weak function of ΔE. The correction is readily calculable from the measured cathode potential and electron current using a density profile in an iterative procedure described by Kilgus *et al.* [17]. Again, the origin of the c.m. energy scale is unaffected by uncertainties in the space-charge correction, but a stretching of the energy scale will occur at the level of the uncertainty of the space-charge correction compared to the cooling energy. We estimate a 5% accuracy of the correction, which leads to an uncertainty of 5×10^{-3} of the relative energy scale in the present case. This uncertainty is further reduced later by a recalibration procedure.

2. Space-charge compensation by slow ions

In principle the space-charge potential can be lowered by the presence of slow positive ions in the electron beam pro-

duced by ionization of residual gas components. In order to extract these ions from the electron beam "clearing" electrodes are mounted at the entrance and the exit of the merging section. They are kept on a negative potential of about 1 keV. However, one has to be aware of the fact that this extraction is not instantaneous because of the limited ion drift velocity. Consequently, one has to expect small deviations of the potential on the electron beam axis from the one expected for a homogeneous electron density distribution. However, the remaining uncertainties in the space-charge potential determination [17] are negligible in the present context.

3. Influence of the toroidal cooler sections

In the toroidal sections of the electron cooler the angle between the electron beam and the ion beam increases with the distance from the straight overlap section. Therefore, the measured rate coefficient at a fixed relative energy contains contributions of higher relative energies [Eq. (3)]. In the experimental setup at the TSR the electron and the ion beam paths through the electron cooler are well known as is the spatial distribution of the magnetic fields. This facilitates an accurate calculation of the toroidal sections' contributions to the measured rate coefficient. The subtraction of these contributions results in a corrected rate coefficient [18] with slightly modified DR resonance line shapes. The accompanying shift in the resonance energies is much less than the uncertainty in the determination of the resonance positions. The corresponding contribution to the uncertainty of the relative energy scale is therefore negligible.

4. Angle between electron and ion beam

When setting up the ion and electron beams one aims at minimizing the angle θ between the two beams. To this end the fact is exploited that the cooling forces exerted by the electron beam on the ion beam are most efficient when both beams are properly centered coaxially on top of each other. Moreover, due to the space-charge effects discussed above the electron velocity is smallest in the center of the electron beam. Therefore, an ion beam of a diameter of a few millimeters centered in the electron beam with a diameter of a few centimeters is dragged to a somewhat lower velocity as compared to an ion beam that traverses the electron beam off center.

Changes in the ion velocity can be sensitively monitored by measuring the distribution of the ion revolution frequencies via an analysis of the Schottky noise [7] generated by the ion beam. The center of the frequency distribution acquires a minimal value when both beams are centered. At the same time the ion beam diameter should become smallest, too. At the TSR the ion beam diameter is measured online by beam profile monitors based on residual gas ionization [19].

With these diagnostic tools at hand a beam alignment of $\theta = 0 \pm 0.2$ mrad is routinely achieved. The 0.2 mrad uncertainty in the angle translates via Eqs. (3) and (4) into an uncertainty of the relative energy scale of 0.1 meV (Table I).

5. Drag force effects

Nonlinear distortions of the energy scale are introduced by drag effects [20]. During the measurement period the electron velocity is changed to achieve a desired E_{rel}. The Coulomb interaction between the electrons and ions now exerts a drag or friction force on the ions trying to pull them to the current electron velocity. This force varies with time since on one hand it depends on the (externally manipulated) relative velocity $\langle v_{\mathrm{rel}} \rangle$ between electrons and ions and on the other hand it influences $\langle v_{\mathrm{rel}} \rangle$. The instantaneous ion velocity $v_i(t)$ at any time of the experiment can be calculated by numerical integration of the differential equation

$$\frac{dv_i}{dt} = \frac{F_{\mathrm{cool}} L}{m_i C}. \tag{7}$$

The cooling force to be inserted into Eq. (7) is known from measurements carried out at the TSR [14] and depends on the relative ion-electron velocity. Since the detuning of the electron energy away from the value E_c at cooling lasts only a few milliseconds (see below) after which the conditions are restored, the much more inert ions are not dragged very far from E_c. As a result from solving Eq. (7) we find that the cooling force produces a shift of the relative energy scale of at most 3.5 meV under the conditions of the present experiment. The energy-dependent shift is applied as a correction to the relative energy scale. It is estimated to be accurate within 50% (Table I).

TABLE I. Breakdown of the uncertainties in the corrected experimental energy scale in the electron-ion c.m frame at $E_{\mathrm{rel}} = 70$ meV. The contributions are added quadratically at the end. The straight sum of all uncertainties is 2.66 meV.

	$\Delta E_{\mathrm{cm}}^{(\mathrm{expt.})}$ (meV)
Beam alignment (±0.2 mrad)	0.10
Remaining uncertainty from drag force	1.7
Energy calibration	0.03
Fitted resonance position	0.30
Uncertainty at zero c.m. energy	0.28
Transverse temperature (±0.5 meV)	0.25
Total	1.8

6. Slew rates of power supplies

This rather technical issue turns out to be the most limiting systematic in the present experiment. For measuring the recombination rate coefficient as a function of relative energy, the electron energy E_e is scanned over a range of preset values by varying the electron cooler's cathode voltage on a millisecond time scale. In detail, the following energy scan scheme was applied in our measurements. In between two measurement steps of 5 ms duration at different nonzero relative energies, the relative energy is first set to zero for a 30 ms cooling period in order to maintain the ion beam quality. Then the recombination rate is monitored for 5 ms at a "reference" energy that is chosen such that the measured "reference" rate coefficient can essentially be interpreted as a background due to charge transfer in collisions of the ions

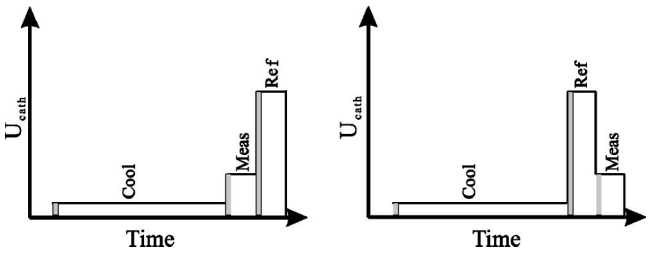

FIG. 2. Schematic picture of the two different data taking modes that were used in the present experiment; the right panel shows mode 1 "Cool-Ref-Meas," indicating the sequence and the duration of scan energies: cooling energy (30 ms), reference energy (5 ms), and measurement energy (5 ms). The left panel shows mode 2 "Cool-Meas-Ref." After each voltage jump a time period of 1.5 ms (gray shaded areas) was allowed for the power supplies to settle in on the new condition before data taking was started. While the voltages in the "Cool" and "Ref" phases of a measurement are fixed the voltage in the "Meas" phase is ramped up or down during a cycle that typically comprises a thousand "Meas" voltages.

with residual gas molecules (see, e.g., [15] for details). As shown in Fig. 2 the order of measurement and reference steps may be interchanged.

The fast variation of the cooler cathode voltage makes the slew rate of the power supplies an issue. The actual cathode voltage is provided by two power supplies, one slow device providing the voltage at cooling and a second, fast, bipolar high-voltage amplifier taking care of the fast jumps. Time-resolved measurements of the voltages have revealed that while the fast supply carries out a voltage jump as ordered, the slow supply "sags" by an amount roughly proportional to the size and the direction of the jump. The recovery time is well beyond the 1.5 ms settling time allowed in the experiment. Waiting, however, at the measuring energy for a much longer time is prohibited by the friction force which immediately starts pulling the ion beam velocity toward the electron velocity. The incomplete recovery of the power supply effectively diminishes the size of the voltage jump by a constant factor. The mismatch either increases or decreases with increasing relative energy depending on whether the mode "Cool-Meas-Ref" or the mode "Cool-Ref-Meas" (Fig. 2), respectively, has been chosen for setting up the voltage ramp. This effect also leads in good approximation to a linear stretching of the c.m. energy scale. This is consistent with the above mentioned behavior of the power supplies. While the origin of this problem is understood, the amount of sagging (up to several percent of E_{rel}) depends on the exact cooler settings and a robust correction does not appear feasible. Instead, we use an experimental calibration of the spectrum.

B. Calibration of the experimental energy scale

Most of the above discussed effects can be corrected for with the remaining errors being small apart from the effect of the finite slew rate of the cathode voltage power supply. In the future a fast feedback system will be implemented at the TSR electron cooler for regulating the cathode voltage to the desired value within ~1 ms. For the time being the experimental energy scale has to be calibrated with the aid of spectral features.

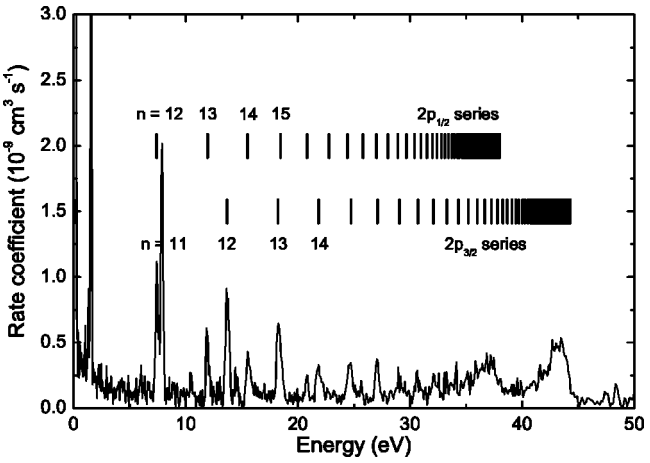

FIG. 3. Absolute Sc^{18+} photorecombination rate coefficients measured as a function of relative energy. The vertical bars indicate the calculated [Eq. (1)] $2p_j n$ DR resonance positions.

In practice the energy-dependent data were first corrected for space-charge effects (Secs. II A 1 and II A 2), toroid contributions (Sec. II A 3), and the influence of drag forces on the ion beam velocity (Sec. II A 5). Then the experimental energy scale was calibrated with the following procedure. In order to fix $E_{\mathrm{rel}}=0$ in the c.m. frame the maximum of the continuous radiative recombination (RR) is used as calibration point. A measurement symmetric to the RR peak provides identical spectral features for "$E_{\mathrm{rel}}<0$" (i.e., the electron velocity is less than the ion velocity) and "$E_{\mathrm{rel}}>0$" (i.e., the electron velocity is greater than the ion velocity). The value for the cooling energy E_c is chosen such that identical peak structures appear at the same absolute values of energy. The resulting cooling energy E_c is accurate to 2.5×10^{-5}, translating to an uncertainty of 0.28 meV at $E_{\mathrm{rel}}=70$ meV (Table I). Two further calibration points are provided by the Sc^{18+} $2s_{1/2}\rightarrow 2p_{1/2}$ and $2s_{1/2}\rightarrow 2p_{3/2}$ excitation energies. In our experimental recombination spectrum (Fig. 3) these two excitation energies correspond to the series limits of $1s^2\,2s+e^-\rightarrow 1s^2\,2p_{1/2,3/2}\,nl$ DR capture series. The series limits cannot be directly observed, as they correspond to capture of the free electron into a fictitious Rydberg state with principal quantum number $n\rightarrow\infty$. Field ionization in the magnets prevents observation of contributions with $n\geqslant n_{cut}=67$. However, individually resolved members of the two $2p_{1/2}nl$ and $2p_{3/2}nl$ series of Rydberg resonances can be used instead. Gaussians were fitted to the $n\geqslant 11$ Rydberg resonances to determine their resonance positions. Due to the linear stretching of the experimental energy scale (Sec. II A 6), the fitted resonance positions have to be corrected with a factor that is determined as follows. For sufficiently high principal quantum numbers n the resonance positions of the Rydberg resonances are well described by Eq. (1) and spacings between consecutive resonances are easy to calculate:

$$a(E_n - E_{n+1}) = Z^2\mathrm{R}\left(\frac{1}{(n+1)^2}-\frac{1}{n^2}\right). \qquad (8)$$

A least squares fitting method determines the scaling factor a, which makes the measured spacings coincide with the

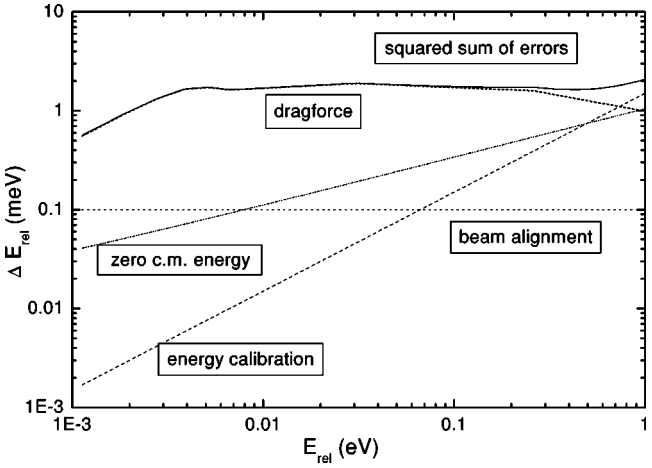

FIG. 4. Uncertainties ΔE_{rel} of the calibrated energy scale as a function of E_{rel}.

corresponding calculated ones. The measured Rydberg resonance energies are corrected with this factor and extrapolated to $n\rightarrow\infty$ using the $1/n^2$ binding energy dependence of Eq. (1). The resulting core excitation energies $E_{1/2}=38.032(19)$eV and $E_{3/2}=44.311(18)$ eV are in good agreement with the literature values of 38.02 and 44.31 eV as determined by emission spectroscopy with an accuracy of ±35 meV [9].

The error from the extrapolation amounts to approximately 20 meV at $E_{\mathrm{rel}}\approx 41$ eV, corresponding to a relative calibration error of 5×10^{-4} and an absolute error of 0.03 meV at $E_{\mathrm{rel}}=70$ meV (Table I). Below the $n=11$ resonance at 3 eV the validity of the linear-stretch correction cannot be experimentally verified. However, there is no reason to expect a different behavior of the power supply in this region. Figure 4 summarizes the energy dependences of the uncertainties associated with the calibrated energy scale of the present measurement.

C. Experimental energy resolution

With regard to spectroscopic resolving power the energy spread of the electron beam in the longitudinal and transversal degrees of freedom is a matter of particular interest. In the frame of the ions the velocity distribution of the electrons can be described by an asymmetric "flattened" Maxwell-Boltzmann distribution characterized by a longitudinal temperature $T_{\parallel}$ and a transverse temperature $T_{\perp}$:

$$f(\vec{v},v_{\mathrm{rel}})=\frac{m_e^{3/2}}{(2\pi k_{\mathrm{B}})^{3/2}T_{\perp}T_{\parallel}^{1/2}}\times\exp\left(-\frac{m_e v_{\perp}^2}{2k_{\mathrm{B}}T_{\perp}}-\frac{m_e(v_{\parallel}-v_{\mathrm{rel}})^2}{2k_{\mathrm{B}}T_{\parallel}}\right),\qquad(9)$$

where $v_{\mathrm{rel}}=\sqrt{2E_{\mathrm{rel}}/m_e}$ is the average longitudinal velocity between the electron and ion ensembles and k_{B} is Boltzmann's constant. In the present experiment the temperatures correspond to thermal energies $k_{\mathrm{B}}T_{\parallel}=0.18(5)$ meV and $k_{\mathrm{B}}T_{\perp}=7.2(5)$ meV (see Sec. IV).

Together with the natural linewidth Γ the total measured full width at half maximum of a resonance amounts to [2]

$$\Delta E=\sqrt{(k_{\mathrm{B}}T_{\perp}\ln 2)^2+16k_{\mathrm{B}}T_{\parallel}E_{\mathrm{rel}}\ln 2+\Gamma^2}.\qquad(10)$$

Evidently, the experimental energy spread is lowest at low relative energies and amounts to $k_{\mathrm{B}}T_{\perp}\ln 2$ for $E_{\mathrm{rel}}\lesssim k_{\mathrm{B}}(\ln 2)T_{\perp}^2/(16\,T_{\parallel})$, i.e., $\Delta E=5$ meV at $E_{\mathrm{rel}}\lesssim 13.5$ meV for the above temperatures of the present experiment. Resonance energies can be determined within a small fraction of the energy spread when the shape of the resonance is known and the measurement has good statistics. In order to exploit this potential the low-energy range of the Sc^{18+} recombination rate coefficient was particularly scrutinized. It should be noted that resonances at energies $E_{\mathrm{rel}}\gg k_{\mathrm{B}}(\ln 2)T_{\perp}^2/(16\,T_{\parallel})$ where the second term in the square root of Eq. (10) dominates the experimental energy spread are not sensitive to the transverse temperature. A reliable determination of $T_{\perp}$ from the shape of a DR resonance is only possible with resonances appearing at low energies. An accurate knowledge of $T_{\perp}$ and $T_{\parallel}$ is essential for precision spectroscopy, especially since the influence of $T_{\perp}$ leads to an asymmetric apparent line profile with its maximum occurring at an energy which is lower than the nominal resonance energy. An uncertainty in the transverse temperature $T_{\perp}$ of ±0.5 meV leads to a possible error of ±0.25 meV at $E_{\mathrm{rel}}=70$ meV. Table I lists all uncertainties contributing to the determination of the resonance energy associated with the peak feature found near 70 meV.

III. THEORETICAL TREATMENT

The first step of dielectronic recombination is taken when the incoming electron excites the target ion and thereby loses enough energy to become bound. The excitation of Sc^{18+} from the ground state to the first excited states requires around 40 eV, which nearly coincides with the binding energy of an $n=10$ electron. We thus expect the lowest-energy recombination resonances to be due to doubly excited states of the form $2p_j10l_{j'}$.

To describe the DR process we need to calculate the energies of the doubly excited states relative to the energy of the ground state of the target ion and the cross section for recombination as a function of energy. We use relativistic many-body perturbation theory in an all-order formulation carried out with complete numerical basis sets, obtained by discretization of the one-particle Hamiltonian on a radial grid in a cavity. There is one basis set for each angular symmetry l_j. Details of the procedure as well as a demonstration of the obtainable accuracy can be found in Ref. [21]. The one-particle Hamiltonian employed here includes the main part of the spherical symmetric potential from the other electrons (see below), while the remaining electron-electron interactions are accounted for through the perturbation expansion. The energy contributions in second order and beyond include in principle an infinite sum over partial waves, which, however, is truncated in the calculations as described below.

Our first step is to calculate the excitation energy in the Li-like Sc^{18+} ion and, in a second step, we calculate the doubly excited states of the Be-like Sc^{17+} ion. The doubly excited states are generally very fragile and decay predomi-

TABLE II. The contributions to the $(2p_{1/2}\text{-}2s_{1/2})$ and $(2p_{3/2}\text{-}2s_{1/2})$ energy splitting in Sc^{18+} in eV.

	$2p_{1/2}\text{-}2s_{1/2}$	$2p_{3/2}\text{-}2s_{1/2}$
Dirac-Fock[a]	38.182 05	44.731 29
Δ Dirac-Fock-Breit[a]	0.257 05	−0.039 18
Retardation beyond Breit[a]	−0.000 81	−0.003 90
Mass polarization[a]	−0.009 76	−0.009 55
All-order correlation (Coulomb+Breit)[a]	−0.171 64(35)	−0.153 44(33)
Total RMBPT	38.256 9(4)	44.525 2(3)
Radiative corrections[b]	−0.230 7(100)	−0.216 3(100)
Total	38.026 1(100)	44.308 9(100)
Experiment (Optical Spectroscopy)[c]	38.02(4)	44.312(35)
Present experiment		44.310 7(19)

[a]A Fermi distribution for the nuclear charge is used.
[b]Y.-K. Kim *et al.* [24]. For a comparison of different calculations see text.
[c]S. Suckewer *et al.* [9].

nantly by autoionization. The resonance strength, i.e., the integrated cross section, is inversely proportional to its position relative to the threshold and proportional to the capture rate into the doubly excited state multiplied with the probability by which the state decays radiatively to a bound state. These quantities are calculated in a third step. In the following we describe the calculation in more detail.

A. The lithiumlike ion

The binding energies of the Sc^{18+} $(1s^2\ 2l_j)$ states calculated with relativistic many-body perturbation theory and with quantum electrodynamical effects taken into account are detailed in Table II where the different contributions to the $2p_{1/2}\text{-}2s_{1/2}$ and $2p_{3/2}\text{-}2s_{1/2}$ splittings in Sc^{18+} are collected. The starting point is the Dirac-Fock result, listed on the first line. On the second line the contribution due to the inclusion of the Breit interaction in the Dirac-Fock potential is shown. Corrections due to retardation beyond the Breit interaction and mass polarization follow on the third and fourth lines. The most important correction is correlation. It is calculated with the coupled-cluster formalism, i.e., with an all-order formulation of perturbation theory where important classes of effects are iterated until convergence is obtained; see e.g., Ref. [22]. For such a highly charged system as Sc^{18+} the dominating correlation contribution enters, however, in second order. The Coulomb correlation contribution to the $2p_{3/2}\text{-}2s_{1/2}$ splitting is, e.g., −158.8 meV, and of this only −1.2 meV comes from correlation beyond second order. The Coulomb and Breit correlation contributions are given together on line five and are dominated by the Coulomb part. The Breit correlation contributes with only 6 meV to the $2p_{3/2}\text{-}2s_{1/2}$ splitting and with less than 1 meV to the $2p_{1/2}\text{-}2s_{1/2}$ splitting. The correlation includes an infinite sum over angular momenta. This sum is here truncated after $l_{\max}=10$. The contribution from higher angular momenta has been estimated by extrapolation which gives the final value, an uncertainty of ≈0.0002 eV. All the RMBPT contributions are calculated in the potential of an extended nucleus with a Fermi distribution of the charge. The critical parameter is the nuclear mean square radius which is estimated by the empirical expression provided in Ref. [23].

The next step is to consider radiative corrections. For H-like systems a detailed tabulation has been compiled by Johnson and Soff [23]. Tabulations have also been presented for Li-like systems by Kim *et al.* [24] and by Blundell [25]. The extensive tabulation by Kim *et al.* has been obtained with the so-called Welton approximation where the hydrogenlike results are scaled with the electron density inside the nucleus to account for screening effects. More recently, first principle calculations have been presented for a range of nuclear charges by Indelicato and Mohr [26] and by Yerokhin *et al.* [27]. Reference [27] shows, however, only results for the $1s^22s_{1/2}$ and $1s^22p_{1/2}$ states. Only the calculation by Kim *et al.* [24] presents explicit results for $Z=21$. We have thus chosen to use their values in Table II. From comparison with the hydrogenlike result by Johnson and Soff [23] the change in the radiative corrections due to the presence of the $1s^2$ core can be deduced. According to Ref. [24] this so-called screening effect is 36.8 meV for the $2p_{1/2}\text{-}2s_{1/2}$ splitting and 31.9 meV for the $2p_{3/2}\text{-}2s_{1/2}$ splitting. The first principle calculation by Yerokhin *et al.* [27] does not tabulate $Z=21$, but after interpolation between listed nuclei we find a screening contribution of 38.4 meV for the $2p_{1/2}\text{-}2s_{1/2}$ splitting, i.e., a deviation from the approximate method by Kim *et al.* of less than 2 meV, or around 5%. The calculation by Indelicato and Mohr [26] also has to be interpolated to obtain results for $Z=21$. Doing this, one finds somewhat bigger screening effects: 51.8 meV for the $2p_{1/2}\text{-}2s_{1/2}$ splitting and 46.7 meV for the $2p_{3/2}\text{-}2s_{1/2}$ splitting. We have no explanation for these differences at present but assign an uncertainty of 10 meV to the radiative corrections in Table II to indicate that this value is still unsettled. A dedicated calculation of the radiative corrections in Sc^{18+} could certainly reduce this uncertainty considerably. The final results for the calculated energy splitting in Sc^{18+} are given in Table II and are also compared with experimental data. Using the calculated $2p_j-2s_{1/2}$ splitting, assuming the validity of Eq. (1), we can estimate the first resonances to appear for $2p_{3/2}10l_j$ doubly excited states. We now proceed to the calculation of the resonances.

B. Resonances in the Be-like ion

The doubly excited states lying above the ionization threshold of Sc^{17+} are of the type $2p_j nl_{j'}$, with $n \geqslant 10$. We concentrate here on the lowest-energy resonances $2p_{3/2}10l_{j'}$. The positions of the resonances are determined by the $2p_{3/2}$-$2s$ splitting and the binding energy of the high-n electron with respect to the excited target. Consequently an accurate calculation of this binding energy can be used to extract the $2p_j$-$2s$ splitting from the experimental determination of the resonance positions relative to the threshold. The high-n state of the outer electron has little overlap with the inner region, diminishing the many-body effects and facilitating the calculational task.

The RMBPT procedure used for the Li-like ion is employed also for the Be-like system, albeit for a situation with two electrons outside closed shells. An important difference is that we now deal with autoionizing states. To handle this we combine RMBPT with *complex rotation*. The latter method facilitates a treatment of decaying states without explicit continuum functions and is today extensively used, combined with various many-body methods. The combination of many-body perturbation theory and complex rotation has earlier been used to describe dielectronic recombination in several Li-like ions (see, e.g., Refs. [5,6,28,29] and references therein).

The starting point for the description of the doubly excited $2p_{3/2}10l_{j'}$ states in the Be-like ion Sc^{17+} is the Dirac-Fock-Breit potential from the $1s^2$ core plus a spherically symmetric potential accounting for the main screening effects by the inner $2p_{3/2}$ electron. The $2p_j10l_{j'}$ configurations are quasidegenerate and are best treated with a perturbation expansion from a so-called extended model space as has been described for Li-like fluorine in Ref. [5]. This means that the mixing among the $2p_j\ 10l_{j'}$ configurations is treated exactly through diagonalization of the Hamiltonian while all other configurations are included perturbatively. The chosen starting point is systematically improved in the perturbation expansion, where correlation due to the Coulomb as well as to the Breit interaction is included. We include all partial waves that contribute when keeping multipoles up to $K=5$ in the partial wave expansion of the interactions. This truncation scheme is more appropriate for states of the type $2p_j\ 10l_{j'}$ with the two valence electrons at very different average distances from the nucleus. The complex rotation calculation gives directly the autoionization width as the imaginary part of the now complex energy.

The accuracy of the calculation is determined by the ability to calculate electron correlation, affecting the obtained energy in second order perturbation theory and beyond. The size of the correlation varies between the resonances and decreases strongly for the high angular momentum states. This is clearly seen in Table III which lists the positions of all the resonances both with a simple (relativistic) hydrogenlike description (second column) of the $n=10$ electron and with a full many-body treatment (third column). For the high-angular-momentum states the difference is very small, often only a few meV; for the lower-angular-momentum states the many-body effects are more significant. Our interest here is primarily to find one, or a few, low-lying and isolated resonances which can be clearly identified in the experiment. The best example found in Table III is the $(2p_{3/2}10d_{3/2})_{J=3}$ resonance at $\sim$0.07 eV. The accuracy possible in the calculation of the binding energy relative to the excited target for this resonance is discussed in detail in Sec. IV below.

C. Recombination cross sections

The integrated cross section, or the strength S, is proportional to the capture rate $A^a_{i\to d}$ into the doubly excited state d, and to the probability of state d decaying radiatively to a nonautoionizing level:

$$S = \int \sigma(\varepsilon_e)d\varepsilon_e = \frac{\hbar^3\pi^2}{2m_e(E_d - E_{ion})}\frac{g_d}{g_i}\frac{A^a_{i\to d}\sum_s A^{\rm rad}_{d\to s}}{A^a + \sum_s A^{\rm rad}_{d\to s}}. \quad (11)$$

The multiplicity of the intermediate doubly excited state is given by g_d and that of the initial target state by g_i, with $g_i=2$ for the Li-like Sc^{18+} ion. $A^a=\Gamma^a/\hbar$ is the total autoionization rate from the doubly excited state d, and $A^{\rm rad}_{d\to s}$ is the radiative transition rate from level d to a level s below the ionization threshold. For field-free conditions the number of bound states that contribute to the stabilization is in principle infinite. In storage-ring experiments the motional electric fields in the magnets will result in field ionization of weakly bound states (see Sec. II), and thus not all recombined ions are detected. Here the magnets prevent observation of contributions with $n \gg n_{\rm cut}=67$. Nevertheless a true high-accuracy calculation of the recombination rates requires highly correlated calculations of a huge number of bound states. Since the systematic experimental uncertainty is 15% and the main interest here is the spectroscopic study, we have chosen to include only stabilization channels that are possible within a one-particle picture. Although these channels are certainly dominating this gives an uncertainty in the resonance strengths which might be of the same order as the systematic experimental uncertainty. The radiative rates from the doubly excited states to bound states are calculated within the dipole approximation. The resonance positions, widths, decay rates, and recombination strengths are listed in Table III. More details about the calculational techniques can be found in Ref. [5].

D. Hyperfine splitting of resonances

At the level of the present experiment's precision hyperfine (hf) splitting of the $2s_{1/2}$ ground state and the $2p_{1/2}$ and $2p_{3/2}$ core excited states becomes noticeable, especially since the nuclear spin of $I=7/2$ of the $^{45}Sc^{18^+}$ isotope is rather large. Boucard *et al.* [30] calculated a hf splitting of 6.0767 meV for the $^{45}Sc^{18^+}$ $(1s^22s_{1/2})$ state and for the $^{45}Sc^{18^+}$ $(1s^22p_{3/2})$ state the total hf splitting has been estimated to amount to about 1.2 meV [31]. Since hf effects are not accounted for in the theoretical methods described above we treat them as modifications that are to be applied to the calculated results presented in Table III. Neglecting the in-

TABLE III. Calculated hydrogenlike energy positions, fully calculated energy positions, the difference between both energies, widths, and strengths for the $Sc^{17+}(2p_{3/2}10l_{j'})$ resonances. The autoionization rate is denoted by A^a and the radiative rate by A^{rad}.

Resonance	Hydrogen (eV)	Position (eV)	Difference (eV)	Width (eV)	A^a (ns^{-1})	A^{rad} (ns^{-1})	Strength (10^{-20} eV cm^2)
$(2p_{3/2}10p_{3/2})_0$	0.1946	0.0342	0.1604	0.0264	40082	129	466
$(2p_{3/2}10d_{3/2})_0$	0.1946	0.1179	0.0767	0.0080	12131	210	217
$(2p_{3/2}10d_{3/2})_1$	0.1946	0.1120	0.0826	0.0057	8688	254	818
$(2p_{3/2}10d_{5/2})_1$	0.2073	0.2148	0.0075	0.0062	9476	226	382
$(2p_{3/2}10f_{5/2})_1$	0.2073	0.2237	0.0164	0.0006	920	103	154
$(2p_{3/2}10d_{3/2})_2$	0.1946	0.0337	0.1609	0.0004	605	245	3211
$(2p_{3/2}10d_{5/2})_2$	0.2073	0.1072	0.1001	0.0038	5829	160	898
$(2p_{3/2}10f_{5/2})_2$	0.2073	0.1893	0.018	0.0002	318	102	252
$(2p_{3/2}10f_{7/2})_2$	0.2136	0.2448	−0.0312	0.0004	580	102	220
$(2p_{3/2}10g_{7/2})_2$	0.2136	0.2343	−0.0207	0.0001	199	59	121
$(2p_{3/2}10d_{3/2})_3$	0.1946	0.0678	0.1268	0.0004	603	283	2463
$(2p_{3/2}10d_{5/2})_3$	0.2073	0.1831	0.0242	0.0038	5732	231	1051
$(2p_{3/2}10f_{5/2})_3$	0.2073	0.1532	0.0541	0.0013	2043	101	542
$(2p_{3/2}10f_{7/2})_3$	0.2136	0.1858	0.0278	0.0002	351	101	366
$(2p_{3/2}10g_{7/2})_3$	0.2136	0.2060	0.0076	<0.0001	39	60	99
$(2p_{3/2}10g_{9/2})_3$	0.2174	0.2391	−0.0217	0.0004	548	60	195
$(2p_{3/2}10h_{9/2})_3$	0.2174	0.2296	−0.0122	0.0002	245	39	126
$(2p_{3/2}10d_{5/2})_4$	0.2073	0.0289	0.1784	0.0003	461	90	2909
$(2p_{3/2}10f_{5/2})_4$	0.2073	0.2058	0.0015	0.0061	9281	99	530
$(2p_{3/2}10f_{7/2})_4$	0.2136	0.1639	0.0497	0.0018	2666	100	655
$(2p_{3/2}10g_{7/2})_4$	0.2136	0.1923	0.0213	0.0019	2836	58	330
$(2p_{3/2}10g_{9/2})_4$	0.2174	0.2084	0.009	<0.0001	55	59	151
$(2p_{3/2}10h_{9/2})_4$	0.2174	0.2127	0.0047	<0.0001	10	39	42
$(2p_{3/2}10h_{11/2})_4$	0.2200	0.2319	−0.0119	0.0002	274	39	163
$(2p_{3/2}10i_{11/2})_4$	0.2200	0.2271	−0.0071	0.0001	111	27	107
$(2p_{3/2}10f_{7/2})_5$	0.2136	0.1827	0.0309	0.0055	8294	102	747
$(2p_{3/2}10g_{7/2})_5$	0.2136	0.2168	−0.0032	0.0072	10922	58	363
$(2p_{3/2}10g_{9/2})_5$	0.2174	0.1962	0.0212	0.0019	2901	58	396
$(2p_{3/2}10h_{9/2})_5$	0.2174	0.2068	0.0106	0.0018	2705	38	248
$(2p_{3/2}10h_{11/2})_5$	0.2200	0.2149	0.0051	<0.0001	58	38	146
$(2p_{3/2}10i_{11/2})_5$	0.2200	0.2169	0.0031	<0.0001	1	27	4
$(2p_{3/2}10i_{13/2})_5$	0.2218	0.2287	−0.0069	0.0001	112	27	130
$(2p_{3/2}10k_{13/2})_5$	0.2218	0.2263	−0.0045	<0.0001	37	20	79
$(2p_{3/2}10g_{9/2})_6$	0.2174	0.2179	−0.0005	0.0071	10856	58	427
$(2p_{3/2}10h_{9/2})_6$	0.2174	0.2207	−0.0033	0.0065	9871	38	278
$(2p_{3/2}10h_{11/2})_6$	0.2200	0.2090	0.011	0.0018	2744	38	290
$(2p_{3/2}10i_{11/2})_6$	0.2200	0.2140	0.006	0.0014	2078	27	201
$(2p_{3/2}10i_{13/2})_6$	0.2218	0.2185	0.0033	<0.0001	7	27	42
$(2p_{3/2}10k_{13/2})_6$	0.2218	0.2196	0.0022	<0.0001	<1	20	<1
$(2p_{3/2}10k_{15/2})_6$	0.2231	0.2275	−0.0044	<0.0001	37	20	93
$(2p_{3/2}10l_{15/2})_6$	0.2231	0.2261	−0.003	<0.0001	9	16	40
$(2p_{3/2}10h_{11/2})_7$	0.2200	0.2229	−0.0029	0.0065	9873	38	318
$(2p_{3/2}10i_{11/2})_7$	0.2200	0.2230	−0.003	0.0048	7344	27	225
$(2p_{3/2}10i_{13/2})_7$	0.2218	0.2156	0.0062	0.0014	2087	27	230
$(2p_{3/2}10k_{13/2})_7$	0.2218	0.2182	0.0036	0.0008	1235	20	169
$(2p_{3/2}10k_{15/2})_7$	0.2231	0.2209	0.0022	<0.0001	6	20	37
$(2p_{3/2}10l_{15/2})_7$	0.2231	0.2216	0.0015	<0.0001	<1	16	1

TABLE III. (*Continued.*)

Resonance	Hydrogen (eV)	Position (eV)	Difference (eV)	Width (eV)	A^a (ns^{-1})	A^{rad} (ns^{-1})	Strength (10^{-20} eV cm^2)
$(2p_{3/2}10l_{17/2})_7$	0.2242	0.2271	−0.0029	<0.0001	9	16	47
$(2p_{3/2}10m_{17/2})_7$	0.2242	0.2263	−0.0021	<0.0001	1	13	8
$(2p_{3/2}10i_{13/2})_8$	0.2218	0.2247	−0.0029	0.0048	7343	27	253
$(2p_{3/2}10k_{13/2})_8$	0.2218	0.2246	−0.0028	0.0028	4268	20	188
$(2p_{3/2}10k_{15/2})_8$	0.2231	0.2194	0.0037	0.0008	1241	20	190
$(2p_{3/2}10l_{15/2})_8$	0.2231	0.2208	0.0023	0.0003	507	16	144
$(2p_{3/2}10l_{17/2})_8$	0.2242	0.2226	0.0016	<0.0001	2	16	20
$(2p_{3/2}10m_{17/2})_8$	0.2242	0.2231	0.0011	<0.0001	<1	12	<1
$(2p_{3/2}10m_{19/2})_8$	0.2250	0.2271	−0.0021	<0.0001	1	12	10
$(2p_{3/2}10k_{15/2})_9$	0.2231	0.2258	−0.0027	0.0028	4283	20	209
$(2p_{3/2}10l_{15/2})_9$	0.2231	0.2254	−0.0023	0.0011	1730	16	162
$(2p_{3/2}10l_{17/2})_9$	0.2242	0.2218	0.0024	0.0003	514	16	161
$(2p_{3/2}10m_{17/2})_9$	0.2242	0.2226	0.0016	0.0001	109	12	118
$(2p_{3/2}10m_{19/2})_9$	0.2250	0.2239	0.0011	<0.0001	1	12	5
$(2p_{3/2}10l_{17/2})_{10}$	0.2242	0.2264	−0.0022	0.0011	1730	16	178
$(2p_{3/2}10m_{17/2})_{10}$	0.2242	0.2258	−0.0016	0.0002	364	12	139
$(2p_{3/2}10m_{19/2})_{10}$	0.2250	0.2234	0.0016	0.0001	110	12	130
$(2p_{3/2}10m_{19/2})_{11}$	0.2250	0.2266	−0.0016	0.0002	364	12	152

teraction of the outer $10l_j$ electron, each of the $2p_{3/2}10l_j$ states is split into hf core levels with total angular momenta ranging from $F'=2$ to $F'=5$. Likewise, the $2s_{1/2}$ ground state is split into two components with $F=3,4$.

The energies of the $2s_{1/2}$ hf components with respect to the nonsplit zero level are −3.42 meV and +2.66 meV for total angular momentum $F=3$ and $F=4$, respectively. An estimate of the lifetime of the upper hf component based on calculations by Beier [32] is of the order of 2500 s, i.e., very much longer than the ion storage times in the experiment. Assuming statistical population of the two hf levels of the ground state is therefore appropriate. The energies of the $2p_{3/2}10l_j$ hf components with respect to the nonsplit zero level are −0.68 meV, −0.38 meV, +0.03 meV, and +0.53 meV for the total angular momenta $F'=2$, $F'=3$, $F'=4$, and $F'=5$, respectively. From these numbers it is apparent that hyperfine effects are dominated by the 6 meV splitting of the $^{45}Sc^{18+}$ $(1s^22s_{1/2})$ ground state. In the DR process resonance strength is distributed among the hf levels of the intermediate excited state in radiationless transitions from the two hf levels of the ground state. This distribution can be regarded as a broadening of the excited level with a shift of the centroid that is only a small fraction of the maximum offset of 0.68 meV of the excited-state hyperfine levels from the undisturbed $2p_{3/2}10l_j$ energy. Hence, with the assumption that the excited levels are not influenced by hyperfine effects the resulting uncertainty of the resonance energies is well below the error bar of 1.8 meV on the experimental energy scale. What remains is the occurrence of resonance doublets resulting from the ground state splitting that share the calculated resonance strength (see Table III) in proportion to their statistical weights, i.e., 7/16 and 9/16.

IV. RESULTS AND DISCUSSION

For a comparison of the calculated RMBPT cross section with the measured spectrum, the former has to be convoluted with the experimental electron velocity distribution function [Eq. (9)]. The comparison is presented in Fig. 5. The electron beam temperatures were taken to be $k_BT_\parallel=0.18(5)$ and $k_BT_\perp=7.2(5)$meV as determined from a fit of DR resonances to the experimental data (see below).

The overall agreement between theory and experiment is quite satisfying. In contrast to the comparison between RMBPT calculation and DR experiment for the lighter lithiumlike F^{6+} ion [5], however, discrepancies are noticeable in the present Sc^{18+} case. The theoretical peak heights below 0.07 eV are by up to 18% larger than the experimental ones. At higher energies they are up to 25% lower. Although these numbers are just outside the 15% systematic experimental uncertainty, the latter cannot fully be made responsible for the observed discrepancy between theory and experiment, since the magnitude of the deviation is energy dependent while the experimental uncertainty results mainly from energy-independent sources. As discussed in Sec. III B the theory introduces additional uncertainties due to the approximations applied to the calculation of rate coefficients.

The strength of the RMBPT calculations is the inclusion of correlation effects to all orders in the determination of level energies. The binding energy of the Rydberg electron in the $1s^2\,2p_j\,nl$ states of the recombined berylliumlike Sc^{17+} ion can therefore be calculated to a much higher degree of accuracy than the $2p_{3/2}$-$2s_{1/2}$ splitting. In combination with a very accurate (±1.8 meV) knowledge of the experimental Sc^{17+} $(1s^22p_{3/2}10l_{j'})$ resonance positions this fact can be exploited for the derivation of an equally accurate value for the

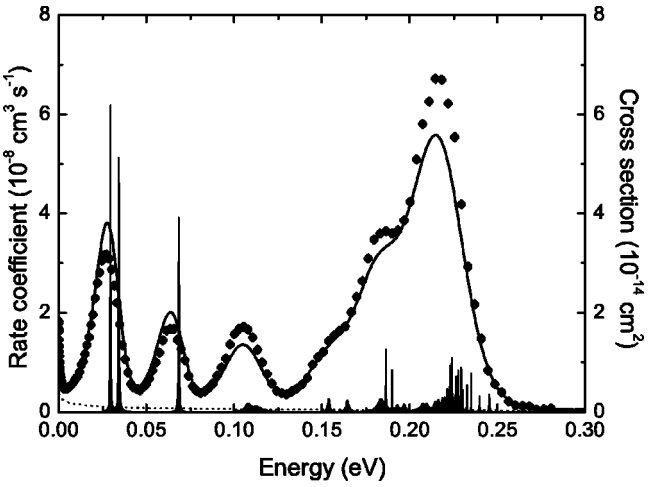

FIG. 5. Comparison of the present RMBPT calculation and the storage-ring experiment on the total photorecombination of Sc^{18+} ions in the energy range of $2p_{3/2}10l_{j'}$ resonances. Experimental rate coefficients are represented by the solid dots. Error bars only slightly larger than the symbol size indicate the statistical uncertainties. The theory-based convoluted product $\langle \sigma v \rangle$ (thick full line) was determined with the temperatures resulting from the analysis in Fig. 6. Calculated background from RR is shown separately (dotted line). The theoretical cross sections show the underlying resonance structure (right hand scale).

$2p_{3/2}$-$2s_{1/2}$ excitation energy as has already been shown by Madzunkov *et al.* [7] for DR of lithiumlike Kr^{33+} ions. The electron-ion collision energy, at which a resonance occurs, is equal to the difference of the core excitation energy and the binding energy of the captured electron:

$$E_{\mathrm{rel}}^{\mathrm{res}} = E_{\mathrm{core\text{-}exc}} - E_{\mathrm{bind}}. \tag{12}$$

As a first guess a (relativistic) hydrogenlike description can be used for the Rydberg electron to obtain E_{bind}. The results obtained for $E_{\mathrm{rel}}^{\mathrm{res}}$ with $q=18$, i.e., assuming full screening of the nucleus by the three inner electrons, are shown in the second column of Table III. These numbers can then be compared with the results of the full calculation shown in the third column. For Rydberg electrons with high angular momenta the difference in energy position is only a few meV. For the lower angular momenta the difference is larger, up to 200 meV, and the issue is now how accurately this part can be calculated. To illustrate this point Table IV lists the different contributions to the binding energy of the isolated resonance at 70 meV. This resonance has total angular momentum $J=3$ and is dominated by the $2p_{3/2}10d_{3/2}$ configuration. We first find the binding energy of the $10d_{3/2}$ orbital in the Dirac-Fock Breit potential from the $1s^2$ core plus the spherically symmetric part of the potential from the $2p_{3/2}$ electron (see Sec. III). The position of the resonance is shifted by nearly 100 meV as compared to the hydrogenlike description. An even further refined treatment of the interaction with the $1s^2$ core, including correlation, changes the binding energy by less than 1 meV.

The next step is to include the full interaction with the $2p_{3/2}$ electron. This is done in two steps. First the full Hamiltonian (with and without the Breit interaction) is diagonalized within the space of the $2p_{3/2}10l_j$ configurations that can couple to $J=3$. In this way we include the first order perturbation from the remaining part of the electron-electron interaction, produce the term splitting, and allow full mixing with, e.g., the $2p_{3/2}10d_{5/2}$ configuration. The result is shown on lines four and five of Table IV. Finally, lines six and seven list the contributions from a second order perturbation treatment, i.e., from correlation between the $2p_{3/2}$ and the $10l_j$ electron. The uncertainty in the calculation comes from this term. We have iterated the interaction between the $2p_{3/2}$ and the $10l_j$ electrons until convergence was reached, i.e., we included correlation to "all orders". The difference compared to second order cannot be seen in Table IV with the number of figures given. We anyhow assign a 0.3 meV uncertainty to the correlation contributions to the binding energy. This uncertainty is calculated by dividing the correlation with the effective charge of the nucleus when screened by three inner electrons ($Z_{\mathrm{eff}}=18$). In this way we should cover uncalculated contributions entering beyond second order.

On the basis of the 0.3 meV uncertainty of the calculated binding energy of the $(2p_{3/2}10d_{3/2})_3$ state (Table IV) and the 1.8 meV uncertainty of the experimental energy scale near $E_{\mathrm{rel}}=70$ meV we can now determine the new value for the $2p_{3/2}$-$2s_{1/2}$ excitation energy by comparing the measured and the calculated spectra. Such comparison is most easily interpreted if an isolated resonance such as the $(2p_{3/2}10d_{3/2})_3$ state is chosen. The uncertainty of the calculated result then depends only on the energy position of that state, and there is no risk that different precision in the calculation of the resonance strengths for a set of unresolved resonances affects the peak position.

TABLE IV. Different contributions to the calculated binding energy of the Rydberg electron in the $(2p_{3/2}10d_{3/2})_{J=3}$ resonance relative to the $2p_{3/2}$ core.

	Individual contribution (eV)	Accumulated sum (eV)
Hydrogenlike description of $10d_{3/2}$	44.114 29	44.1143
Dirac-Fock description of $10d_{3/2}$	0.0099 63	44.2139
Correlation between $10d_{3/2}$ and the $1s^2$ core	0.000 86	44.2148
Full $2p_{3/2}10l_j$ Coulomb interaction first order	0.020 45	44.2353
Full $2p_{3/2}10l_j$ Breit interaction first order	0.000 03	44.2353
Coulomb correlation second order	0.005 76(30)	44.2411(3)
Breit correlation second order	0.000 04	44.2411(3)

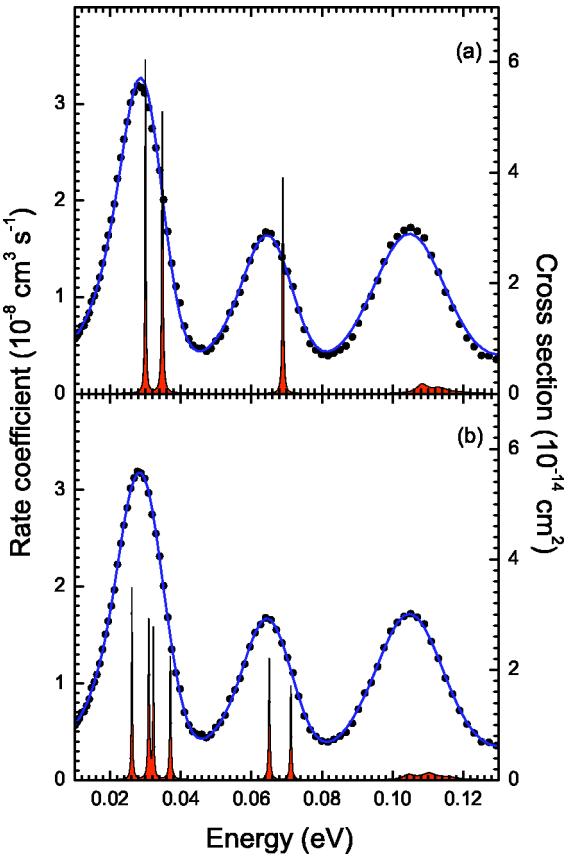

FIG. 6. Fit of theoretical DR resonances to the experimental data. The resonance positions were allowed to vary (see text). In (b) hyperfine effects are additionally taken into account.

For the purpose of energy and temperature determination a fit of theoretical resonance features to the experiment in the energy range from 0 to 0.13 eV (Fig. 6) was carried out. However, the resonance parameters predicted by theory were allowed to vary to some extent—keeping in mind that only three peak features are resolved in the investigated energy range. These peak features are associated with three groups of resonances, where the second group at about 70 meV consists of the hyperfine components of the $(2p_{3/2}10d_{3/2})_3$ state. In the fit, variable strengths and variable centroid energies were allowed for each resonance group while the natural widths, the relative positions, and the relative strengths of individual resonances within each group were kept fixed at the theoretical values. In the fit also the electron beam temperatures were allowed to vary. The quantities obtained, $k_BT_{\parallel}=0.18(5)$ meV and $k_BT_{\perp}=7.2(5)$ meV, were already used above as an input for generating the theoretical recombination rate coefficients shown in Fig. 5.

As compared to Fig. 5 the fit shows much improved agreement with the experimental data [Fig. 6(a)]. The agreement is even better when the hyperfine splitting of the resonances into doublets (as described in Sec. III D) is taken into account [Fig. 6(b)]. The hf splitting of 6.0767 meV and the relative weights of the two resonances in each doublet are retained in the fit while—as before—variable strengths and variable centroid energies were allowed for each resonance group.

With the precision accomplished by the present experiment, it is now possible to derive the $2p_{3/2}$-$2s_{1/2}$ excitation energy. As mentioned above, the best candidate for calibrating the theoretical energy scale to the experiment is the isolated resonance at about 70 meV. It is a single hyperfine-split resonance from which the experimental resonance energy can be determined without additional ambiguity. The fitted value of the $(2p_{3/2}10d_{3/2})_3$ resonance energy measured from the undisturbed ground state is 69.6 ± 0.3 meV, i.e., 1.8 meV above the theoretical result which was obtained from the (relatively uncertain) $2p_{3/2}$-$2s_{1/2}$ excitation energy of 44.3089 ± 0.10 eV and the precise binding energy of 44.2411 ± 0.0003 eV. Combining the experimental resonance energy with the calculated binding energy of the $(2p_{3/2}10d_{3/2})_3$ state provides a new improved $2p_{3/2}$-$2s_{1/2}$ excitation energy of 44.3107 ± 0.0019 eV. The total uncertainty of 1.9 meV results from the quadrature sum of the uncertainties of the binding energy, of the resonance-energy fit, and of the experimental energy scale (cf. Table I). Within the experimental error bars our value agrees with the hitherto most precise spectroscopic value for the $2p_{3/2}$-$2s_{1/2}$ excitation energy 44.312(35) eV [9], but is almost a factor of 20 more accurate.

V. SUMMARY AND CONCLUSIONS

Electron-ion recombination of lithiumlike Sc^{18+} $(1s^2\ 2s)$ at very low c.m. energies produces DR resonances associated with $1s^2\ 2p_{3/2}\ 10l_{j'}$ states which straddle the Sc^{17+} ionization threshold and range up to 0.3 eV. In this energy range, merged-beam experiments at storage rings have an excellent energy resolution and therefore are sensitive to fine details in the cross sections. Accordingly, the reproduction of experimental findings by theory requires very elaborate high-quality calculations. The present RMBPT approach provides results which are in almost perfect agreement with the experiment as far as resonance energies are considered. Differences of up to 25% are observed between theoretical and experimental heights of individual resonance features. However, the integral over the theoretical rate-coefficient curve describing the $n=10$ Rydberg resonance manifold is only 5.6% below the experiment. The accuracy of the experimental energy scale after the calibration is characterized by an uncertainty of 1.8 meV at the position of the lowest-energy resonances. With this precision a value for the $2p_{3/2}$-$2s_{1/2}$ splitting in Sc^{18+} was derived [44.3107(19)eV] that is more than one order of magnitude more accurate than the previously published value from optical spectroscopy.

In spite of the present improvement in the determination of the excitation energy for Sc^{18+} to a relative uncertainty of 43 ppm the state-of-the-art precision of optical measurements has barely been matched. Relative uncertainties of the most accurate $2p_{3/2}$-$2s_{1/2}$ transition energies measured with emission-spectroscopy methods reach down as far as 22 ppm for Cr^{21+} [33], i.e., for an ion not far from scandium in the lithium isoelectronic sequence. The absolute uncertainty in that case was only 1.2 meV compared to the 1.9 meV uncertainty of the present result. The record accuracy for $2p_{3/2}$-$2s_{1/2}$ transition energies of highly charged Li-like ions

is presently held by an emission-spectroscopy experiment on Bi^{80+} with a relative uncertainty of only 14 ppm [34]. On an absolute scale the uncertainty in that experiment is 39 meV which is about a factor 20 above the absolute error bars of the present study. While the absolute uncertainty of optical measurements increases with the energy of the observed line, the uncertainty of the present technique is independent of the transition energy studied. In principle, recombination spectroscopy can result in uncertainties as low as about 1 meV even for the most highly charged ions, provided that low-energy resonances are available. One example for that is the analysis of a measurement on Pb^{53+} [10] where a relative uncertainty of 8.5 ppm was achieved for a transition in a multielectron system.

We consider the present work as one important step in the development of an alternative method that is competitive with emission spectroscopy. Our analysis shows that storage-ring recombination experiments bear the potential of much higher accuracy than that achieved in the present study. This is particularly interesting for the determination of excitation energies in very highly charged heavy ions, also including high charge states of radioactive isotopes with lifetimes reaching down into the range of minutes. In the present case, the drag force effects and the statistics of the experimental results were the limiting factors in the accuracy achieved on the $2p_{3/2}$-$2s_{1/2}$ excitation energy. Both factors can be pushed to lower limits in future experiments.

ACKNOWLEDGMENTS

We thank the MPIK accelerator and storage ring teams for their support. This research was partially funded by BMBF, Bonn, through Contract No. 06 GI 848; and DFG, through Contracts No. Mu 1068/8-1 and No. Mu 1068/8-2.

[1] A. Müller and A. Wolf, in *Accelerator-Based Atomic Physics Techniques and Applications*, edited by J. C. Austin and S. M. Shafroth (AIP Press, Woodbury, NY, 1997), p. 147.
[2] A. Müller, Philos. Trans. R. Soc. London, Ser. A **357**, 1279 (1999).
[3] G. Gwinner *et al.*, Phys. Rev. Lett. **84**, 4822 (2000).
[4] S. Mannervik, D. deWitt, L. Engström, J. Lidberg, E. Lindroth, R. Schuch, and W. Zong, Phys. Rev. Lett. **81**, 313 (1998).
[5] M. Tokman *et al.*, Phys. Rev. A **66**, 012703 (2002).
[6] W. Zong, R. Schuch, E. Lindroth, H. Gao, D. R. DeWitt, S. Asp, and H. Danared, Phys. Rev. A **56**, 386 (1997).
[7] S. Madzunkov, E. Lindroth, N. Eklöw, M. Tokman, A. Paál, and R. Schuch, Phys. Rev. A **65**, 032505 (2002).
[8] C. Brandau *et al.*, Phys. Rev. Lett. **91**, 073202 (2003).
[9] S. Suckewer, J. Cecci, S. Cohen, R. Fonck, and E. Hinnov, Phys. Lett. **80A**, 259 (1980).
[10] E. Lindroth, H. Danared, P. Glans, Z. Pesic, M. Tokman, G. Vikor, and R. Schuch, Phys. Rev. Lett. **86**, 5027 (2001).
[11] M. Grieser, M. Blum, D. Habs, R. V. Hahn, B. Hochadel, E. Jaeschke, C. M. Kleffner, M. Stampfer, M. Steck, and A. Noda, in *Proceedings of the 19th International Symposium on Cooler Rings and Their Applications, Tokyo, Japan, 1990*, edited by T. Katayama and A. Noda (World Scientific, Singapore, 1991), pp. 190–198.
[12] H. Danared, Nucl. Instrum. Methods Phys. Res. A **335**, 397 (1993).
[13] H. Danared *et al.*, Phys. Rev. Lett. **72**, 3775 (1994).
[14] S. Pastuszka *et al.*, Nucl. Instrum. Methods Phys. Res. A **369**, 11 (1996).
[15] S. Schippers, T. Bartsch, C. Brandau, A. Müller, G. Gwinner, G. Wissler, M. Beutelspacher, M. Grieser, A. Wolf, and R. A. Phaneuf, Phys. Rev. A **62**, 022708 (2000).
[16] G. Miersch, D. Habs, J. Kenntner, D. Schwalm, and A. Wolf, Nucl. Instrum. Methods Phys. Res. A **369**, 277 (1996).
[17] G. Kilgus, D. Habs, D. Schwalm, A. Wolf, N. R. Badnell, and A. Müller, Phys. Rev. A **46**, 5730 (1992).
[18] A. Lampert, A. Wolf, D. Habs, J. Kenntner, G. Kilgus, D. Schwalm, M. S. Pindzola, and N. R. Badnell, Phys. Rev. A **53**, 1413 (1996).
[19] B. Hochadel, F. Albrecht, M. Grieser, D. Habs, D. Schwalm, E. Szmola, and A. Wolf, Nucl. Instrum. Methods Phys. Res. A **343**, 401 (1994).
[20] W. Shi *et al.*, Phys. Rev. A **66**, 022718 (2002).
[21] S. Salomonson and P. Öster, Phys. Rev. A **40**, 5548 (1989).
[22] I. Lindgren and J. Morrison, *Atomic Many-Body Theory*, 2nd ed., Series on Atoms and Plasmas (Springer, New York, 1986).
[23] W. R. Johnson and G. Soff, At. Data Nucl. Data Tables **33**, 405 (1985).
[24] Y.-K. Kim, D. H. Baik, P. Indelicato, and J. P. Desclaux, Phys. Rev. A **44**, 148 (1991).
[25] S. A. Blundell, Phys. Rev. A **46**, 3762 (1992).
[26] P. Indelicato and P. J. Mohr, Phys. Rev. A **63**, 052507 (2001).
[27] V. A. Yerokhin, A. N. Artemyev, T. Beyer, G. Plunien, V. M. Shabaev, and G. Soff, Phys. Rev. A **60**, 3522 (1999).
[28] P. Glans, E. Lindroth, N. R. Badnell, N. Eklöw, W. Zong, E. Justiniano, and R. Schuch, Phys. Rev. A **64**, 043609 (2001).
[29] E. Lindroth, Hyperfine Interact. **114**, 219 (1998).
[30] S. Boucard and P. Indelicato, Eur. Phys. J. D **8**, 59 (2000).
[31] I. I. Sobelman, *Atomic Spectra and Radiative Transitions* (Springer, Berlin, 1992).
[32] T. Beier, Habilitationsschrift, Technische Universität Dresden, Dresden, 2000.
[33] J. Sugar, V. Kaufman, and W. L. Rowan, J. Opt. Soc. Am. B **10**, 13 (1993).
[34] P. Beiersdorfer, A. L. Osterheld, J. H. Scofield, J. R. Crespo López-Urrutia, and K. Widman, Phys. Rev. Lett. **80**, 3022 (1998).